JACS
JOURNAL OF THE AMERICAN CHEMICAL SOCIETY

Communication

pubs.acs.org/JACS

Hierarchically Assembled Theranostic Nanostructures for siRNA Delivery and Imaging Applications

Ritu Shrestha,[†] Mahmoud Elsabahy,*[,†,∥] Hannah Luehmann,[§] Sandani Samarajeewa,[†] Stephanie Florez-Malaver,[†] Nam S. Lee,[†,⊥] Michael J. Welch,[§,‡] Yongjian Liu,*[,§] and Karen L. Wooley*[,†]

[†]Department of Chemistry, Department of Chemical Engineering, and Laboratory for Synthetic-Biologic Interactions, Texas A&M University, P.O. Box 30012, College Station, Texas 77842, United States

[§]Department of Radiology, Washington University, Saint Louis, Missouri 63110, United States

[∥]Department of Pharmaceutics, Faculty of Pharmacy, Assiut University, Assiut, Egypt

Supporting Information

ABSTRACT: Dual functional hierarchically assembled nanostructures, with two unique functions of carrying therapeutic cargo electrostatically and maintaining radiolabeled imaging agents covalently within separate component building blocks, have been developed via the supramolecular assembly of several spherical cationic shell cross-linked nanoparticles clustered around a central anionic shell cross-linked cylinder. The shells of the cationic nanoparticles and the hydrophobic core domain of the anionic central cylindrical nanostructure of the assemblies were utilized to complex negatively charged nucleic acids (siRNA) and to undergo radiolabeling, respectively, for potential theranostic applications. The assemblies exhibited exceptional cell transfection and radiolabeling efficiencies, providing an overall advantage over the individual components, which could each facilitate only one or the other of the functions.

Construction of sophisticated three-dimensional multifunctional nanostructures, such as viruses, in Nature by sequential hierarchical assembly of simpler lower order building blocks (i.e., amino acids to proteins to viral capsid assembly) provides broad inspiration[1,2] and has prompted us to expand our synthetic methodology for the preparation of nanoscopic discrete objects from molecular polymerization and macromolecular assembly to the next level of complexity, involving the hierarchical assembly of nanoscopic building blocks. From a fundamental perspective, the development of strategies to construct unique objects in the laboratory setting from nanoscopic materials is of interest to explore advantageous effects of their compositions, structures, overall shapes, and internal morphologies on their biological interactions and properties. Ultimately, multiple levels and types of functional performance may be incorporated. With recent advances in nanotechnologies, a high level of attention is being directed toward the creation of polymeric nanoobjects that can bring together multiple components, for instance to achieve coincident therapy and diagnosis in nanomedicine applications.

Several nanomedical objects incorporate multiple functions within a single entity, where optimization for the integration of various functionalities into nanoparticles plays a critical role in their performance and biological behavior *in vivo*. Current methods for introduction of multifunctionalities involve manipulation of polymers that are the building blocks of the nanoparticles, which can be iterative and inefficient, as entirely new block copolymers must be synthesized to alter the composition of merely one element contributing to the multifunctionality. Recently, the combination of multiple functions through several individual nanoscopic units is receiving increased attention, due to the potential for simplification and individualized optimization. As an example, Bhatia et al. recently reported the employment of two different nanoparticles in tandem, with each performing a different function to achieve increased drug delivery for the treatment of breast cancer.[3] First, a gold nanorod "scout" nanoparticle was administered, to accumulate at the tumor site and initiate a clotting cascade after being heated by infrared light irradiation. The clotting process produced additional signals for attracting a second type of nanoparticle loaded with doxorubicin, which led to a 40-fold increase in the amount of drug delivered into the tumor, relative to control studies. Such "division of labor" allows versatility of each of the nanoparticles to be adjusted for their individual performance for a mutually enhanced function and behavior *in vivo*.

In our continued interest in exploring nanoscopic objects designed for various biomedical applications, shell cross-linked knedel-like nanoparticles (SCKs) with tunable size, shape, and morphology have been extensively investigated.[4−11] These SCKs consist of a hydrophobic core and a hydrophilic shell domain, the latter of which can be modified to carry radionuclides, poly(ethylene glycol)s (PEGs), targeting moieties, fluorophore labels, and various payloads to serve as vehicles for combinational therapies. Herein, we have adopted an intermediate approach to bring together individual components with unique properties by hierarchical assembly of the independent units. Hierarchical assembly of two different modules, one loaded with therapeutic cargo and the other with sites to carry imaging agents, was achieved by templating cationic SCKs (cSCKs) that can electrostatically bind negatively charged siRNA onto anionic shell cross-linked rods (SCRs), the core of which provides sites for radiolabeling.

Received: July 18, 2012
Published: October 10, 2012

   dx.doi.org/10.1021/ja306616n | J. Am. Chem. Soc. 2012, 134, 17362−17365

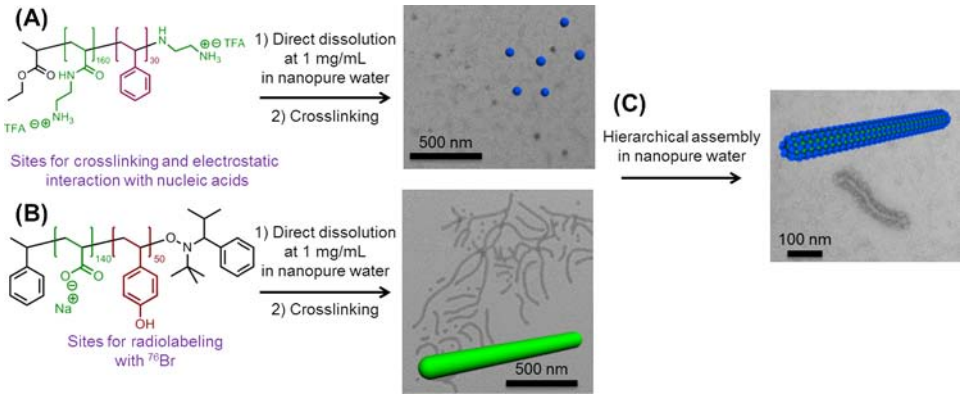

Figure 1. (A) Preparation of cSCKs by directly dissolving polymers into water to obtain micelles followed by cross-linking selectively in the shell region. (B) Preparation of anionic nanorods by directly dissolving polymers followed by cross-linking in the shell region. (C) Hierarchical assembly of cSCKs on SCRs via supramolecular assembly in aqueous medium.

These hierarchically assembled theranostic (HAT) nanostructures hold great potential as a platform that allows for merging individual components with independent domains for carrying payloads and radiolabels, optimized as agents for combined therapy and diagnosis.

Our initial focus is on the construction of multifunctional nanomaterials that present surface chemistries for transport of nucleic acids as therapeutic cargo into cells, while also possessing an overall shape that provides for long *in vivo* lifetimes. In our laboratory, these have included spherical cSCKs, which have been shown to package negatively charged nucleic acids via electrostatic interactions, protect them from enzymatic degradation, and deliver them into cellular target sites.[9,10] However, many reports of the effects of nanoparticle structure on *in vivo* pharmacokinetics have shown that high aspect ratio nanoparticles provide for extended blood circulation lifetimes,[12,13] while the cell internalization kinetics are dependent on the size, shape, and also surface chemistry.[14,15] Although those studies have focused on negatively charged or neutral materials, examples of cylindrical or rod-shaped nanomaterials having cationic surface characteristics have been produced by engineering[16,17] or block copolymer crystallization-driven supramolecular assembly approaches.[18] We have demonstrated that the cSCK property of cell transfection can be transferred onto nanocylinders upon co-assembly,[19] and therefore, in our effort to extend those initial studies to fully functional high aspect ratio nanostructures capable of nucleic acids delivery with radiolabel tracking, we have explored, as an alternative approach, hierarchical supramolecular assemblies of cSCKs, produced together with negatively charged SCRs, which have sites for radiolabeling in the core.

The cSCKs were prepared in a two-step process, first by direct dissolution of poly(acrylamidoethylamine)$_{160}$-*block*-polystyrene$_{30}$ (PAEA$_{160}$-*b*-PS$_{30}$) to obtain a micellar solution that underwent selective cross-linking of 5% of the amines within the hydrophilic shell domain by employing a diacid cross-linker, 4,15-dioxo-8,11-dioxa-5,14-diazaoctadecane-1,18-dioic acid (activated using *O*-benzotriazole-*N*,*N*,*N*′,*N*′-tetramethyl-uronium hexafluorophosphate (HBTU) and hydroxybenzotriazole (HOBT) in DMF), in aqueous medium (Figure 1A and Supporting Information (SI)-S1). Dynamic light scattering and transmission electron microscopy (TEM) were used to determine the sizes of the particles in solution and in the dry state to be ∼20 and 15 nm (n = 100), respectively. A zeta potential value of ∼35 mV was determined by electrophoretic light scattering measurements, indicating that the surface of the cationic nanoparticles was positively charged.

Similarly, anionic cylinders were prepared by aqueous self-assembly and shell cross-linking of the amphiphilic block copolymer poly(acrylic acid)$_{140}$-*block*-poly(*p*-hydroxystyrene)$_{50}$ (PAA$_{140}$-*b*-P*p*HS$_{50}$), as reported previously,[20] that consisted of PAA as the hydrophilic shell segments and P*p*HS as the hydrophobic core domain (SI-S2). The cylindrical micelles were allowed to undergo cross-linking of ∼10% of the acrylic acid residues by amidation with the amine groups of the cross-linker (2,2′-ethylenedioxy)bis(ethylamine) in the presence of 1-ethyl-3-(3′-dimethylaminopropyl)carbodiimide methiodide (Figure 1B). TEM images confirmed that these nanostructures were rod-like with diameters of ∼10 nm and lengths of ∼1.5 μm (n = 100). Zeta potential measurements were used to evaluate the surface charge of the nanorods, which was found to be −30 mV, indicating that they were negatively charged.

The individual cationic spherical and anionic cylindrical nanostructures were co-assembled and further assessed for their performances *in vitro*. The hierarchical assemblies were prepared by mixing cationic spheres with anionic cylinders in aqueous medium at an amine-to-carboxylate (N/C) ratio of 10:1. The surfaces of the nanorods were coated with the spheres, as demonstrated by TEM imaging (Figure 1C, SI-S3 and Figure S1). Zeta potential measurements of the complexes were ∼25 mV, indicating a decrease in the net charge of the spheres as a result of electrostatic complexation to the negatively charged cylinders, although still maintaining a net positive charge. The abilities of these supramolecular structures to complex siRNA onto the PAEA shell of the spheres and to carry ^{76}Br radiolabels in the P*p*HS core of the cylinders were investigated next.

Binding of siRNA to the individual components and to the HAT nanoassemblies was studied, followed by evaluating the transfection efficiencies of the siRNA nanocomplexes in two different cancer cell lines. Cylindrical nanoparticles, cSCKs, and HAT nanostructures were mixed with Cy3-labeled siRNA, and their binding efficiencies were studied by agarose gel electrophoresis at various amine-to-phosphodiester (N/P) ratios (Figure 2). Both the cSCKs and the assemblies were able to completely bind the siRNA at a N/P ratio of 2, indicating that the hierarchical assembly process did not adversely affect the electrostatic interactions between cSCKs and nucleic acids. The percentages of free (noncomplexed) siRNA at N/P ratios of 0.5

dx.doi.org/10.1021/ja306616n | *J. Am. Chem. Soc.* 2012, 134, 17362−17365

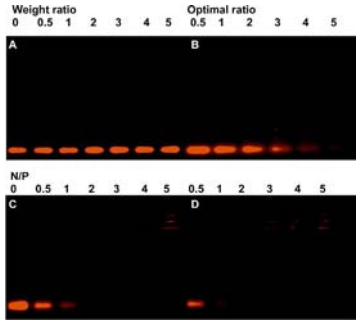

Figure 2. Gel-shift assay of Cy3-labeled siRNA, either naked, mixed with the cylinders (A) or Lipofectamine (B), or complexed to cSCKs (C) or HAT (D) at increasing N/P, weight, or optimal ratios.

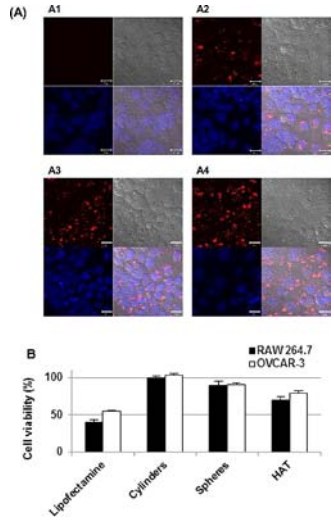

Figure 3. (A) LSCM images of OVCAR-3 cells that were treated with Cy3-labeled siRNA (200 nM) mixed with cylinders (A1) or complexed with Lipofectamine (A2), spherical cSCKs (A3), or HAT (A4) for 3 h. The Cy3-siRNA and the nucleus stained with DRAQ-5 appear in the red (upper left) and blue (lower left) panels, respectively. The light-transmitted images (upper right) and merged images (lower right) are also presented. (B) Transfection efficiency of the cell-death siRNA (100 nM) mixed with the cylinders or complexed to Lipofectamine, spherical cSCKs, or HAT nanostructures.

and 1 were 66 vs 62% and 39 vs 20% of the control siRNA for the spherical cSCKs and HAT nanostructures, respectively (Figure 2C,D). These data indicate the ability of both cSCKs and HAT nanostructures to complex siRNA, with slightly higher efficiency for the HAT, probably due to the cooperative electrostatic interactions between the multiple spheres assembled on the surface of the cylinders, as compared to the individual spherical cSCKs. On the contrary, the anionic cylinders were not able to complex the siRNA at a weight ratio up to 5 (cylinders to siRNA; because the anionic cylinders lack amino groups, except for the few that may be present due to incomplete reaction of the cross-linker, a N/P ratio was not applicable), due to the lack of positively charged functionalities, which are required for siRNA complexation (Figure 2A). It is worth mentioning that the amount of cylinders utilized at a weight ratio of 0.5 is higher than the amount of cylinders incorporated into the HAT at a N/P ratio of 5, indicating that the anionic cylinders did not contribute to the binding property of the HAT, but probably clustering of multiple cationic spheres on their surfaces enhanced the electrostatic binding efficiencies with siRNA. In the case of Lipofectamine, complete binding was not observed even at 5-fold the amount recommended by the manufacturer, whereas complete binding of the same amount of siRNA was observed at a N/P ratio of 2 for the cSCKs and HAT (Figure 2B). The latter demonstrates the advantage of using nanoparticles for the efficient complexation of nucleic acids, in particular for *in vivo* applications, where complete shielding from extra- and intracellular nucleases is essential for increasing the delivery of intact siRNA to the target sites. For further studies, the nanocomplexes were prepared at a N/P ratio of 5.

The cellular uptake and transfection efficiencies of the Cy3-labeled siRNA as mixtures/complexes with cylinders, cSCKs, HAT assemblies, and Lipofectamine were studied by laser scanning confocal microscopy (LSCM) in human ovarian adenocarcinoma (OVCAR-3) cells (Figure 3). Both cSCKs and assemblies showed comparable cellular uptake (Figure 3A3,A4) that was higher than that of Lipofectamine (Figure 3A2), as indicated by the visual fluorescence intensities and the apparent number of fluorescent cells in the images. No uptake was observed in the control (untreated) cells (data not shown) or cells treated with a mixture of siRNA/cylinders (Figure 3A1), which is in agreement with the gel-shift assay results (Figure 2). siRNA cell death assay was then performed using OVCAR-3 cancer cells and RAW 264.7 mouse macrophages (Figure 3B), by measuring the relative viabilities of cells treated with nanoparticles loaded with siRNA that induces cell death vs the cells treated with the same nanoparticles but loaded with a negative control siRNA. The nanoparticles showed lower transfection efficiency than Lipofectamine. Our group and others have shown that cellular uptake is not always correlated with transfection efficiency.[4,21] The lower transfection of nanoparticles might be related to the higher stability of the complexes that partially retard the release of siRNA intracellularly. For instance, Leroux and co-workers have found that amine-functionalized poly(glycerol methacrylate) linear polymer induced higher bcl-2 oncoprotein knockdown as compared to the star-shaped analogue, although the latter demonstrated higher antisense oligonucleotide binding efficiency.[22] In both cell lines, HAT assemblies induced higher cell death (transfection) as compared to the cSCKs, and, as expected, no transfection was found for the death-siRNA mixed with the cylinders. The difference in transfection between the cSCKs and the HAT might be related to the multivalent binding of the HAT structures to the cell surface, which allowed a longer contact period for the intracellular delivery of siRNA. Further studies of the intracellular delivery mechanisms of the cSCKs and assemblies are currently underway.

To further evaluate their potential as theranostic candidates, these nanoparticles were incubated with 130 μCi ^{76}Br in phosphate-buffered saline (PBS) with the addition of bromoperoxidase (0.6 unit) in hydrogen peroxide (2.65 pmol) for 1 h at 0 °C. The radiochemical purities of ^{76}Br-radiolabeled nanoparticles were monitored by radio instant thin-layer chromatography. Among the three nanoparticles, SCRs had the highest radiolabeling yield (94%) and specific activity (SA = 6.06 μCi/μg) (Figure 4), which was comparable to the SA of other phenolic-containing nanostructures.[23] Hierarchical assembly by surrounding the anionic SCRs with cSCKs diminished the radiolabeling capability only slightly, giving a radiolabeling yield of 72% and SA = 4.69 μCi/μg. As expected, the PS core-containing cSCKs gave the lowest

dx.doi.org/10.1021/ja306616n | J. Am. Chem. Soc. 2012, 134, 17362−17365

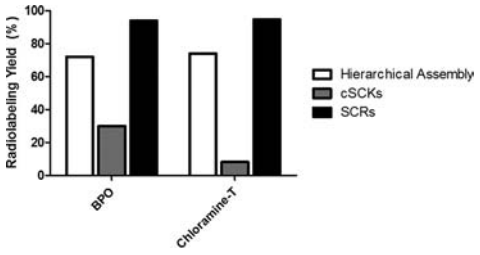

Figure 4. Radiolabeling of nanostructures using ^{76}Br. The nanostructures were incubated with 130 μCi ^{76}Br in 1× PBS with the addition of bromoperoxidase (0.6 unit) in hydrogen peroxide (2.65 pmol) for 1 h at 0 °C and chloramine-T (219.6 nmol) at room temperature for 1 h, respectively.

radiolabeling yield, 30% and SA = 2.01 μCi/μg. Additionally, the chloramine-T method was also used for radiobromination of the three types of nanoparticles, and the labeling results were similar to those obtained by the bromoperoxidase method (Figure 4).

In summary, we have prepared HAT nanostructures where cationic spheres, for complexation of siRNA as a therapeutic cargo, were templated around anionic cylinders with sites for radiolabeling in their hydrophobic cores. These nanostructures were able to efficiently complex siRNA and deliver it intracellularly. The HAT structures showed superior siRNA binding affinity and transfection efficiency, in comparison to the individual cationic spheres and anionic cylinders. Additionally, they were radiolabeled with ^{76}Br and exhibited superior radiolabeling efficiency as compared to the cSCK samples. The HAT nanostructures constitute the first steps toward the development of novel materials that can take advantage of individual components and serve as the next generation of theranostic agents.

■ ASSOCIATED CONTENT

Ⓢ Supporting Information

Detailed experimental procedures. This material is available free of charge via the Internet at http://pubs.acs.org.

■ AUTHOR INFORMATION

Corresponding Author

wooley@chem.tamu.edu; liuyo@mir.wustl.edu; mahmoud.elsabahy@chem.tamu.edu

Present Address

[⊥]Dow Electronic Materials, The Dow Chemical Company, Marlborough, MA 01752

Notes

The authors declare no competing financial interest.

[‡]Deceased, May 6, 2012.

■ ACKNOWLEDGMENTS

We acknowledge financial support from the National Institutes of Health, National Heart Lung and Blood Institute, as a Program of Excellence in Nanotechnology (HHSN268201000046C), the National Institute of Diabetes and Digestive and Kidney Diseases (R01-DK082546), and the Welch Foundation W. T. Doherty-Welch Chair in Chemistry, Grant No. A-0001. The authors also thank Hasitha Samarajeewa and Adriana Pavia for graphics. This work is dedicated to the memory of Dr. Michael J. Welch.

■ REFERENCES

(1) Zhang, S. G. *Nat. Nanotechnol.* **2006**, *1*, 169−170.
(2) Whitesides, G. M.; Grzybowski, B. *Science* **2002**, *295*, 2418−2421.
(3) von Maltzahn, G.; Park, J. H.; Lin, K. Y.; Singh, N.; Schwoppe, C.; Mesters, R.; Berdel, W. E.; Ruoslahti, E.; Sailor, M. J.; Bhatia, S. N. *Nat. Mater.* **2011**, *10*, 545−552.
(4) Shrestha, R.; Elsabahy, M.; Florez-Malaver, S.; Samarajeewa, S.; Wooley, K. L. *Biomaterials* **2012**, *33*, 8557−8568.
(5) Samarajeewa, S.; Shrestha, R.; Li, Y. L.; Wooley, K. L. *J. Am. Chem. Soc.* **2012**, *134*, 1235−1242.
(6) Shrestha, R.; Shen, Y. F.; Pollack, K. A.; Taylor, J. S. A.; Wooley, K. L. *Bioconjugate Chem.* **2012**, *23*, 574−585.
(7) Sorrells, J. L.; Shrestha, R.; Neumann, W. L.; Wooley, K. L. *J. Mater. Chem.* **2011**, *21*, 8983−8986.
(8) Nystrom, A. M.; Wooley, K. L. *Acc. Chem. Res.* **2011**, *44*, 969−978.
(9) Elsabahy, M.; Wooley, K. L. *Chem. Soc. Rev.* **2012**, *41*, 2545−2561.
(10) Elsabahy, M.; Wooley, K. L. *J. Polym. Sci., Polym. Chem.* **2012**, *50*, 1869−1880.
(11) Cui, H. G.; Chen, Z. Y.; Zhong, S.; Wooley, K. L.; Pochan, D. J. *Science* **2007**, *317*, 647−650.
(12) Geng, Y.; Dalhaimer, P.; Cai, S. S.; Tsai, R.; Tewari, M.; Minko, T.; Discher, D. E. *Nat. Nanotechnol.* **2007**, *2*, 249−255.
(13) Decuzzi, P.; Godin, B.; Tanaka, T.; Lee, S. Y.; Chiappini, C.; Liu, X.; Ferrari, M. *J. Controlled Release* **2010**, *141*, 320−327.
(14) Cho, E. C.; Au, L.; Zhang, Q.; Xia, Y. *Small* **2010**, *6*, 517−522.
(15) Zhang, K.; Rossin, R.; Hagooly, A.; Chen, Z.; Welch, M. J.; Wooley, K. L. *J. Polym. Sci., Polym. Chem.* **2008**, *46*, 7578−7583.
(16) Doshi, N.; Mitragotri, S. *J. R. Soc. Interface* **2010**, *7*, S403−410.
(17) Gratton, S. E. A.; Ropp, P. A.; Pohlhaus, P. D.; Luft, J. C.; Madden, V. J.; Napier, M. E.; DeSimone, J. M. *Proc. Natl. Acad. Sci. U.S.A.* **2008**, *105*, 11613−11618.
(18) Petzetakis, N.; Dove, A. P.; O'Reilly, R. K. *Chem. Sci.* **2011**, *2*, 955−960.
(19) Zhang, K.; Fang, H.; Li, Z.; Ma, J.; Hohlbauch, S. V.; Taylor, J. S. A.; Wooley, K. L. *Soft Matter* **2009**, *5*, 3585−3589.
(20) Lee, N. S.; Lin, L. Y.; Neumann, W. L.; Freskos, J. N.; Karwa, A.; Shieh, J. J.; Dorshow, R. B.; Wooley, K. L. *Small* **2011**, *7*, 1998−2003.
(21) Elsabahy, M.; Wazen, N.; Bayo-Puxan, N.; Deleavey, G.; Servant, M.; Damha, M. J.; Leroux, J. C. *Adv. Funct. Mater.* **2009**, *19*, 3862−3867.
(22) Gao, H.; Elsabahy, M.; Giger, E. V.; Li, D. K.; Prud'homme, R. E.; Leroux, J. C. *Biomacromolecules* **2010**, *11*, 889−895.
(23) Almutairi, A.; Rossin, R.; Shokeen, M.; Hagooly, A.; Ananth, A.; Capoccia, B.; Guillaudeu, S.; Abendschein, D.; Anderson, C. J.; Welch, M. J.; Frechet, J. M. J. *Proc. Natl. Acad. Sci. U.S.A.* **2009**, *106*, 685−690.